Breast cancer cells grown on hyaluronic acid-based scaffolds as 3D in vitro model for electroporation

Bioelectrochemistry 136 (2020) 107626

Contents lists available at ScienceDirect

Bioelectrochemistry

journal homepage: www.elsevier.com/locate/bioelechem

Breast cancer cells grown on hyaluronic acid-based scaffolds as 3D *in vitro* model for electroporation

Elisabetta Sieni [a,*], Bianca Bazzolo [b], Fabio Pieretti [c], Annj Zamuner [c], Alessia Tasso [b], Monica Dettin [c], Maria Teresa Conconi [b]

[a] Department of Theoretical and Applied Sciences, University of Insubria, Via Dunant, 3, 21100 Varese, Italy
[b] University of Padova, Department of Pharmaceutical and Pharmacological Sciences, 35131 Padova, Italy
[c] University of Padova, Department of Industrial Engineering, Via Marzolo, 9, 35131 Padova, Italy

ARTICLE INFO

Article history:
Received 22 January 2020
Received in revised form 30 July 2020
Accepted 30 July 2020
Available online 1 August 2020

Keywords:
Electroporation
Breast cancer
Hyaluronic acid
Self-assembling peptides
IKVAV adhesion motif

ABSTRACT

Nowadays, electroporation (EP) represents a promising method for the intracellular delivery of anticancer drugs. To setting up the process, the EP efficiency is usually evaluated by using cell suspension and adherent cell cultures that are not representative of the *in vivo* conditions. Indeed, cells are surrounded by extracellular matrix (ECM) whose composition and physical characteristics are different for each tissue. So, various three-dimensional (3D) *in vitro* models, such as spheroids and hydrogel-based cultures, have been proposed to mimic the tumour microenvironment.

Herein, a 3D breast cancer *in vitro* model has been proposed. HCC1954 cells were seeded on crosslinked and lyophilized matrices composed of hyaluronic acid (HA) and ionic complementary self-assembling peptides (SAPs) already known to provide a fibrous structure mimicking collagen network. Herein, SAPs were functionalized with laminin derived IKVAV adhesion motif. Cultures were characterized by spheroids surrounded by ECM produced by cancer cells as demonstrated by collagen1a1 and laminin B1 transcripts. EP was carried out on both 2D and 3D cultures: a sequence of 8 voltage pulses at 5 kHz with different amplitude was applied using a plate electrode. Cell sensitivity to EP seemed to be modulated by the presence of ECM and the different cell organization. Indeed, cells cultured on HA-IKVAV were more sensitive than those treated in 2D and HA cultures, in terms of both cell membrane permeabilization and viability. Collectively, our results suggest that HA-IKVAV cultures may represent an interesting model for EP studies. Further studies will be needed to elucidate the influence of ECM composition on EP efficiency.

1. Introduction

Electrochemotherapy (ECT) is a well-known therapy combining the chemotherapy with the local electroporation (EP) of cell membranes [1,2]. A multiple needle electrode is locally implanted and energized by a sequence of square voltage pulses 100 μs long [3,4]. The electric field generated at a suitable amplitude permeabilizes the cell membrane thus enhancing the drug uptake. ECT is currently used in clinical practice to treat some types of skin tumors (such as melanoma), and chest wall recurrences of breast cancer [4–7]. Since promising results were obtained on skin metastasis where complete local response rates ranged from 50% to 90% [5], a lot of efforts have been pursued to apply this technique to other tumours such as e.g. sarcomas, bone metastasis, liver and pancreatic tumours [8–12].

Nowadays, two-dimensional (2D) *in vitro* models comprising cells grown as monolayers or in suspension are widely used to set up ECT conditions and evaluate its effectiveness [13–19]. However, these approaches do not fully resemble tumour microenvironment since they lack cell-cell and cell-extracellular matrix (ECM) interactions [20–25]. It has been shown that ECM plays a fundamental and detrimental role in tumour progression: it is dynamically remodelled to support tumour growth and metastasis [26]. Moreover, several studies carried out by means of numerical models and phantoms have shown that the heterogeneity of the tissue influences the local electric field intensity [27–30].

Given the importance of the ECM, three-dimensional (3D) *in vitro* models have been developed to generate culture systems

* Corresponding author.
E-mail addresses: elisabetta.sieni@uninsubria.it (E. Sieni), bianca.bazzolo@studenti.unipd.it (B. Bazzolo), fabio.pieretti@unipd.it (F. Pieretti), annj.zamuner@unipd.it (A. Zamuner), monica.dettin@unipd.it (M. Dettin), mariateresa.conconi@unipd.it (M.T. Conconi).

https://doi.org/10.1016/j.bioelechem.2020.107626
1567-5394/

resembling the tumour microenvironment [31–33]. Up to now, 3D-MultiCellular Tumour Spheroids (3D-MCTSs) represent one of the best characterized model and have been used to study ECT [34–36]. MCTSs show some favourable features: a relative ease of self-assembly, the possibility to co-culture cancer and stromal cells (thus mimicking tumour cell heterogeneity), and reproducibility [37]. However, not all cell lines are able to generate spheroids and even though cells in MCTSs can synthetize some components of their ECM, this system exhibits low amount of ECM components as well as few cell-ECM interactions [25]. Therefore, several efforts have been made to obtain 3D models reproducing the complexity of the tumour ECM. In this context, several materials from natural resources, such as hyaluronic acid (HA), as well as synthetic polymers, like poly lactic acid and polycaprolactone, or decellularized tissues have been used [38–41]. The scaffold-based cultures could provide both a physiological context to cancer cells and the critical biological and mechanical cues needed to maintain morphological and genotypic tumorigenicity [42]. These models have been used used in EP and ECT studies as reliable platform to simulate the *in vivo* environment [36,38,41,43–46].

In our previous works, scaffolds composed of HA and ionic complementary self-assembling peptides functionalized with IKVAV adhesion motif have been proposed [47,48]. Our data have shown that these scaffolds induced the proliferation of human breast adenocarcinoma MCF7 cells and the production of fibrous ECM components.

HA, a glycosaminoglycan (GAG) composed of a repeating disaccharide (glucuronic acid and N-acetyl- glucosamine (b1,4-GlcUA-b1,3-GlcNAc-)n), is an abundant component of the ECM in tumours with myxoid stroma [25]. It is involved in cancer progression and over-expressed in breast cancer compared to normal breast tissue [26]. Self-assembling peptides (SAPs) are able to autonomously organize into ordered structures thanks to hydrogen bonds, van der Waals, and ionic interactions [49]. They are composed of 16 residue sequences with alternating hydrophilic/hydrophobic amino acids and a pattern characterized by 2 negative/2 positive charges. In aqueous solution, SAPs form β-sheets: one side presents hydrophobic residues, whereas on the opposite side the presence of positive and negative charges gives hydrophilic features. So, β-sheets can interact each other and generate hydrogel with multilayered structure. The first SAP was the EAK peptide, discovered by Zhang in 1993 [50] and containing alanin (Ala) as hydrophobic amino acid. Herein, EAbuK peptide, carrying 2-aminobutyric acid instead of Ala, was conjugated with the laminin-derived adhesion motif IKVAV, which has been shown to be involved in tumorigenesis and metastasis [51].

In this work, breast cancer HCC1954 cells were seeded on lyophilized scaffolds composed of HA and SAPs carrying IKVAV adhesion sequence. Cultures were characterized at various time points (1, 3, and 7 days from seedings): cell morphology, cell growth, and matrix deposition were evaluated by means of phase contrast microscopy, cell viability, histochemical staining, immunofluorescence and mRNA expression analysis. Then after, EP was carried out on selected HA-based cultures and cell permeabilization and viability were compared to that obtained on 2D cultures.

2. Material and methods

2.1. Materials

Hyaluronic acid (MW = 100–1250 kDa) was obtained from Contipro Biotech s.r.o (Dolni Dobrouc, Czech Republic). 1-Ethyl-3-(3-dimethylaminopropyl)carbodiimide (EDC), Triethoxysilane (TES), and bovine serum albumin (BSA) from Sigma Aldrich (Steinheim, Germany), and ethanol from VWR Chemicals Prolab (Fontenay-sous-Bois, France). The Rink Amide MBHA resin and the Fmoc protected amino acids were purchased from Novabiochem (Merck KGaA, Darmstadt, Germany). The coupling reagents 2-(1H-Benzotriazole-1-yl)-1,1,3,3-tetramethyluronium hexafluorophosphate (HBTU) and 1-Hydroxybenzotriazole (HOBt) from Advanced Biotech (Seveso, MI, Italy). *N*,*N*-diisopropylethylamine (DIEA) and piperidine were purchased from Biosolve (Leenderweg, Valkenswaard, The Netherlands). *N*,*N*-dimethylformamide (DMF), trifluoroacetic acid (TFA), *N*-methyl-2-pyrrolidone (NMP) and dichloromethane (DCM) were from Biosolve (Leenderweg, Valkenswaard, The Netherlands). Acetonitrile, TFA, propidium iodide (PI), Hoechst 33,342 (HOE) were from Sigma-Aldrich. The HCC1954 cells line was purchased by ATTC (Guernsey, UK). Fetal bovine serum (FBS), culture media and supplements were obtained from Corning (Mediatech Inc., USA). The PrestoBlue™ Cell Viability Reagent, and secondary antibody goat anti-mouse Alexa 488 were purchased by Thermo Fisher Scientific (Eugene, Oregon, USA), whereas Masson's trichrome staining kit by BioOptica (Milan, Italy). The RNeasy mini Kit was purchased by Qiagen (Crawley, UK), the qPCRBIO SyGreen 1-Step Go Lo-ROX by PCRBIOSYSTEMS (London, UK), and Gel Red Nucleic Acid staining by Biotium (Hayward, California, USA). Anti-laminin B1 sc-374015 antibody was provided by Santa Cruz (Dallas, Texas, USA), and Fluoroshield with DAPI from Vector Laboratories (Peterborough, UK).

2.2. Preparation of the scaffolds

The self-assembling peptide with IKVAV adhesive motif was synthesized by Fmoc chemistry using Rink Amide MBHA resin (0.7 mmol/g; scale 0.125 mmol) and the synthesizer Syro I (Multisynthec, Witten, Germany). The first three amino acids and the last sixteen amino acids were introduced through double couplings. At the end of the synthesis, the Fmoc was removed, the

Table 1
Primers for PCR amplification.

Gene	Primer sequence
GAPDH	F- TCTTCCAGGAGCGAGATC
	R- CAGAGATGATGACCCTTTTG
Collagen 1a1 (Col1a1)	F- GACTGGTGAGACCTGCGTGT
	R- TTGTCCTTGGGGTTCTTGCT
Laminin B1 (LamB1)	F- GCGAGAATCCCAGTTCAAGG
	R- GGGGTGTTCCACAGGTCATT

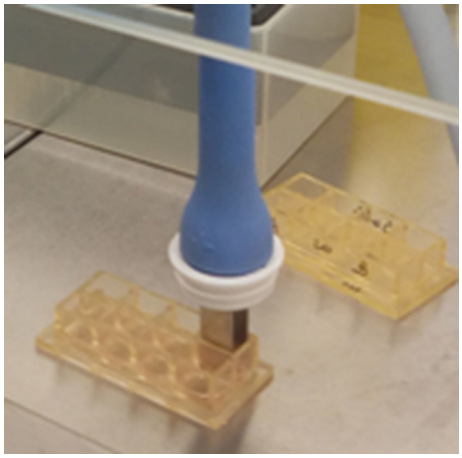

Fig. 1. Electroporation set-up.

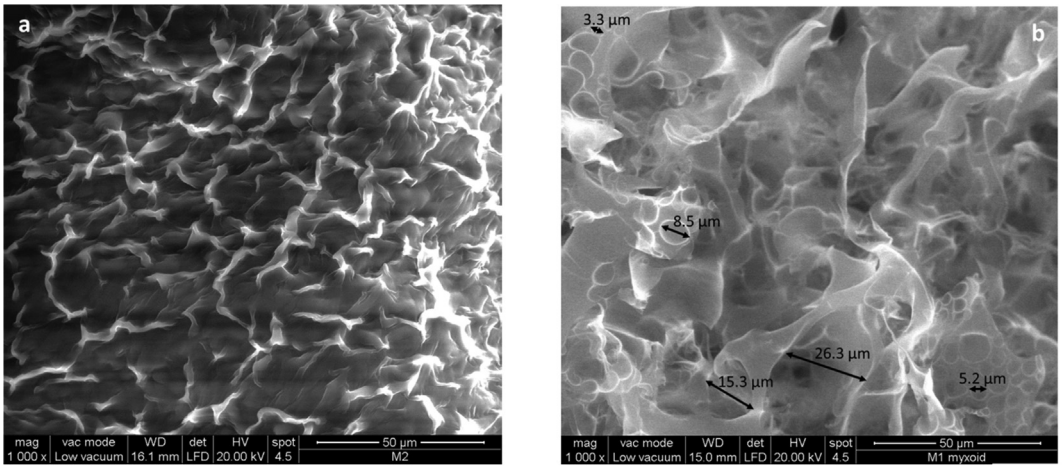

Fig. 2. ESEM micrographs of HA (a) and HA-IKVAV (b) dry scaffolds without cells. Bar: 50 μm. Arrows indicate dimensions of some scaffold pores.

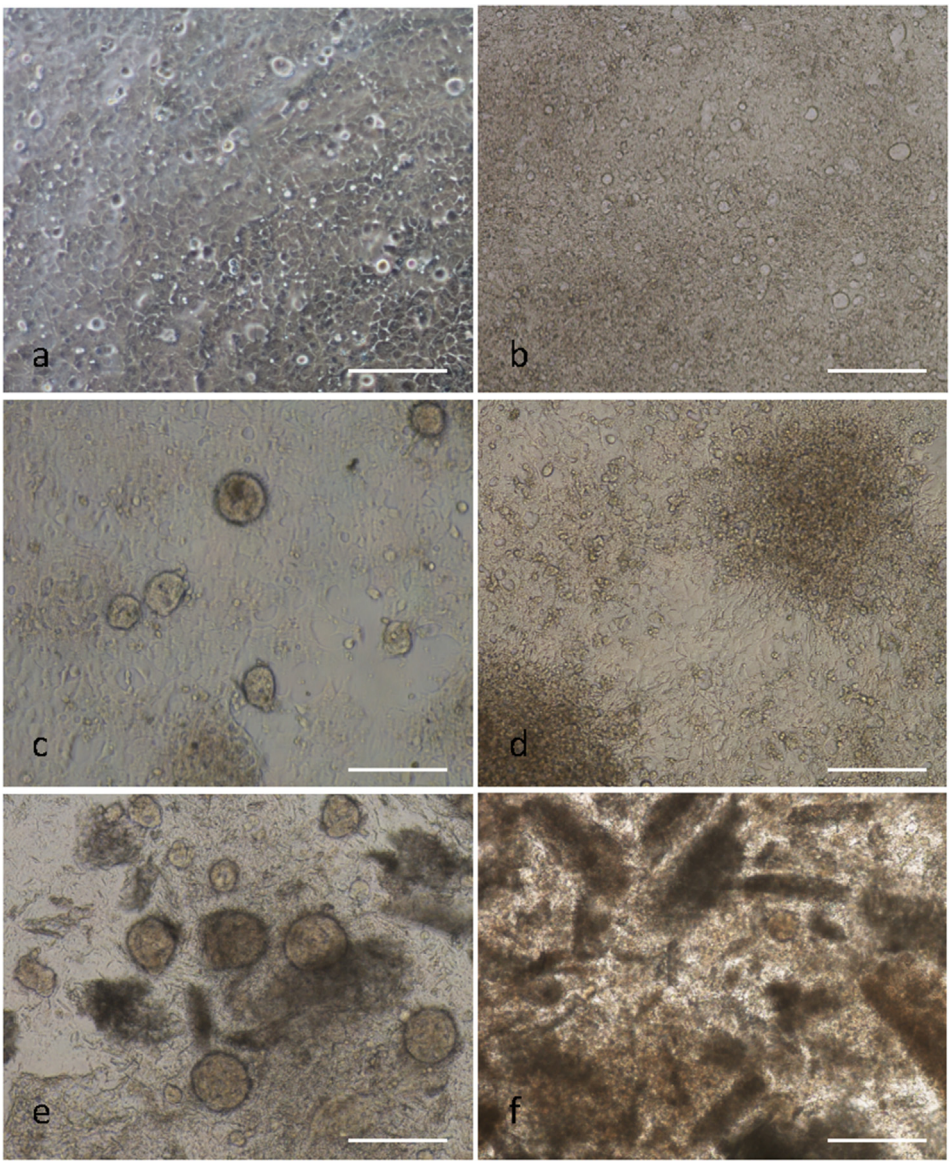

Fig. 3. Phase contrast microscopy of cultures grown on tissue-culture polystyrene (a,b), HA (c,d) and HA-IKVAV (e,f) scaffolds at 3 (a,c,e) and 7 (b,d,f) days from seeding. Bar: 200 μm.

resin was washed with DCM and dried for 1 h under vacuum. The peptide was cleaved from the solid support with contemporary side-chain deprotection using the following mixture: 0.125 mL MilliQ water, 0.125 mL TES, and 4.750 mL TFA over 90 min, under magnetic stirring. The resin was filtered, and the reaction mixture was concentrated. The crude peptide was precipitated with cold diethyl ether. The peptide was purified by RP-HPLC and its identity was ascertained by MALDI-TOF mass spectrometry (theoretical value = 2239 Da; experimental value = 2236,32 Da) [52].

HA-based scaffolds containing self-assembling peptides functionalized with IKVAV adhesion motif (HA-IKVAV) were prepared as follows: SAP (4.2 mg, 0.12% w/v) was dissolved in 3.5 mL of MilliQ water under stirring. HA (108 mg, 3% w/v) was slowly added to the solution. The dense solution was divided into the 5 wells of a chamber slide, frozen in liquid nitrogen and lyophilized. The scaffolds (dimension: 8 × 10 × 5 mm) were cross-linked through reaction with 50 mM EDC in 95% ethanol for 24 h. The scaffolds were washed in an ultrasound bath twice with ethanol for 30 sec and twice with MilliQ water for 30 sec. Finally, the scaffolds were frozen at −20 °C and lyophilized. To obtain HA-based scaffold (HA; control) without peptide the same procedure described before was used without SAP addition.

Hydrated scaffolds were analyzed through the Environmental Scanning Electron Microscope (ESEM) Quanta 200 (FEI, Hillsboro, OR, USA).

2.3. Cell cultures

HCC1954 cells (derived from human ductal carcinoma cells, primary tumour) were cultured in RPMI supplemented with 1% penicillin/streptomycin, 1% L-glutamine, and 10% FBS at 37 °C in a humified atmosphere with 5% CO_2 (SteriCult CO_2 incubator, Thermo Electron Corporation). Cells ($2x10^5$) were seeded on hydrated scaffolds previously put in each well of a 24-well cell suspension culture plate. Cultures were daily observed with a phase contrast microscope (Nikon T-s). At 1, 3, and 7 d from seeding, cell viability was assessed by using the PrestoBlue™ Cell Viability Reagent according to the manufacturer's instruction. Briefly, at each time point 10% PrestoBlue™ was added to each well and incubated for 30 min at 37 °C. Fluorescence (excitation 560 nm emission 590 nm) was read using the Victor^3 1420 Multilabel Counter (PerkinElmer). Fluorescence values derived from blank, containing PrestoBlue and medium, were subtracted from those referred to cell cultures. Sphere diameters and number were determined on 10 phase-contrast micrographs (magnification x200, field area = 291445 μm^2) using ImageJ tools. At 3 and 7 d from seeding, samples were put on a slide and fixed with 4% formaldehyde. To detect collagen production, Masson's trichrome staining was carried out. Quantification of collagen-positive area was carried out on 10 random fields (magnification x200, field area = 291445 μm^2) for each sample using ImageJ tools.

2.4. Reverse transcription polymerase chain reaction (RT-PCR)

At 3 days from seeding, total RNA was extracted using RNeasy mini Kit according to the manufacturer's instructions and quantified using NANODROP 2000 (Thermo Scientific). Primers were obtained from Invitrogen and their sequences are reported in Table 1. GAPDH was chosen as the housekeeping gene. RT-PCR was carried out through the qPCRBIO SyGreen 1-Step Go Lo-ROX according to manufacturer's protocol and using total RNA at concentration of 75 ng/reaction for each sample. The thermal cycling program consisted of 50 °C for 10 min (reverse transcription), 95 °C for 2 min (DNA-polymerase activation), 40 two-step cycles of 95 °C for 5 sec (denaturation), 62 °C for 25 sec (annealing and elongation). The procedure was carried out using the C1000 Touch thermal cycler (Bio Rad). The PCR products were separated by 1% agarose gel electrophoresis and visualized by Gel Red Nucleic Acid staining 1:10,000. The images of the gel were captured with Gel Doc™ Imager (Bio-Rad) and analysed with Image Lab software (Bio-Rad). To obtain a semiquantitative assessment of gene expression, normalized ratios were obtained by comparing the integrated density values for target genes with those for GAPDH. Then, results were expressed as percentage from control cultures taken as 100%.

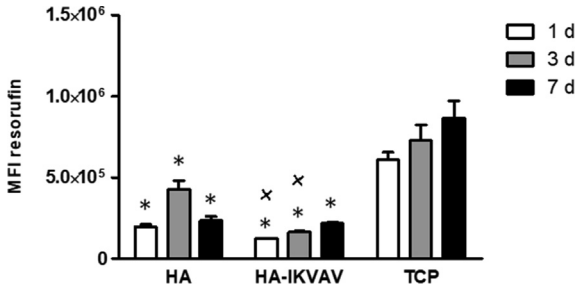

Fig. 4. Cell viability at various time points from seeding. MFI: mean fluorescence intensity. * = p < 0.05 vs corresponding cultures grown on tissue-culture polystyrene (TCP). x = p < 0.05 vs corresponding cultures grown on HA scaffolds.

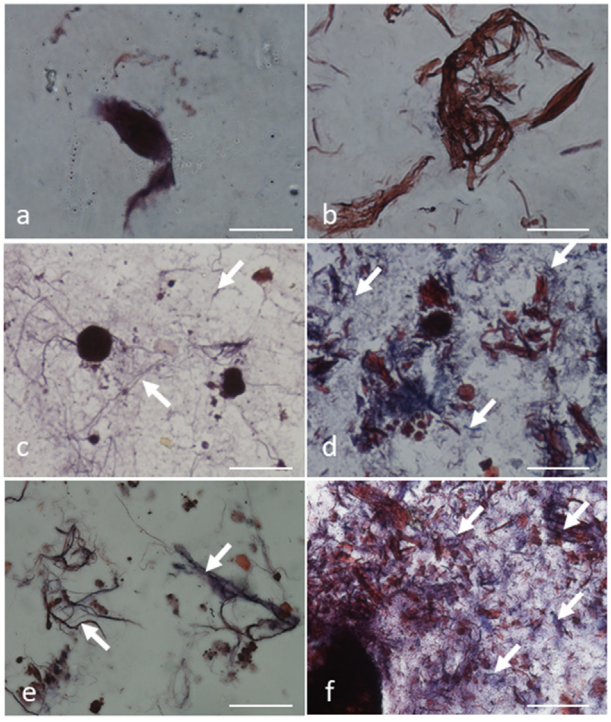

	Collagen positive areas (μm²)
HA 3d	5,2 ± 1,9
HA IKVAV 3d	13,2 ± 5,9 *
HA 7d	14,2 ± 4,4
HA IKVAV 7d	30,6 ± 5,9 *

Fig. 5. Masson's trichrome staining of cultures grown on HA (a,c,e) and HA-IKVAV (b,d,f) scaffolds at 3 (c,d) and 7 (e,f) d from seeding. The corresponding scaffolds without cells and hydrated for 3 d are reported in a and b. Collagen stains blue, cytoplasm red and nuclei black. Bar: 100 μm. White arrows indicate collagen fibers. Table reports the quantification of blue-stained areas carried out by ImageJ tools. * = p < 0.05 vs corresponding cultures grown on HA scaffolds. (For interpretation of the references to colour in this figure legend, the reader is referred to the web version of this article.)

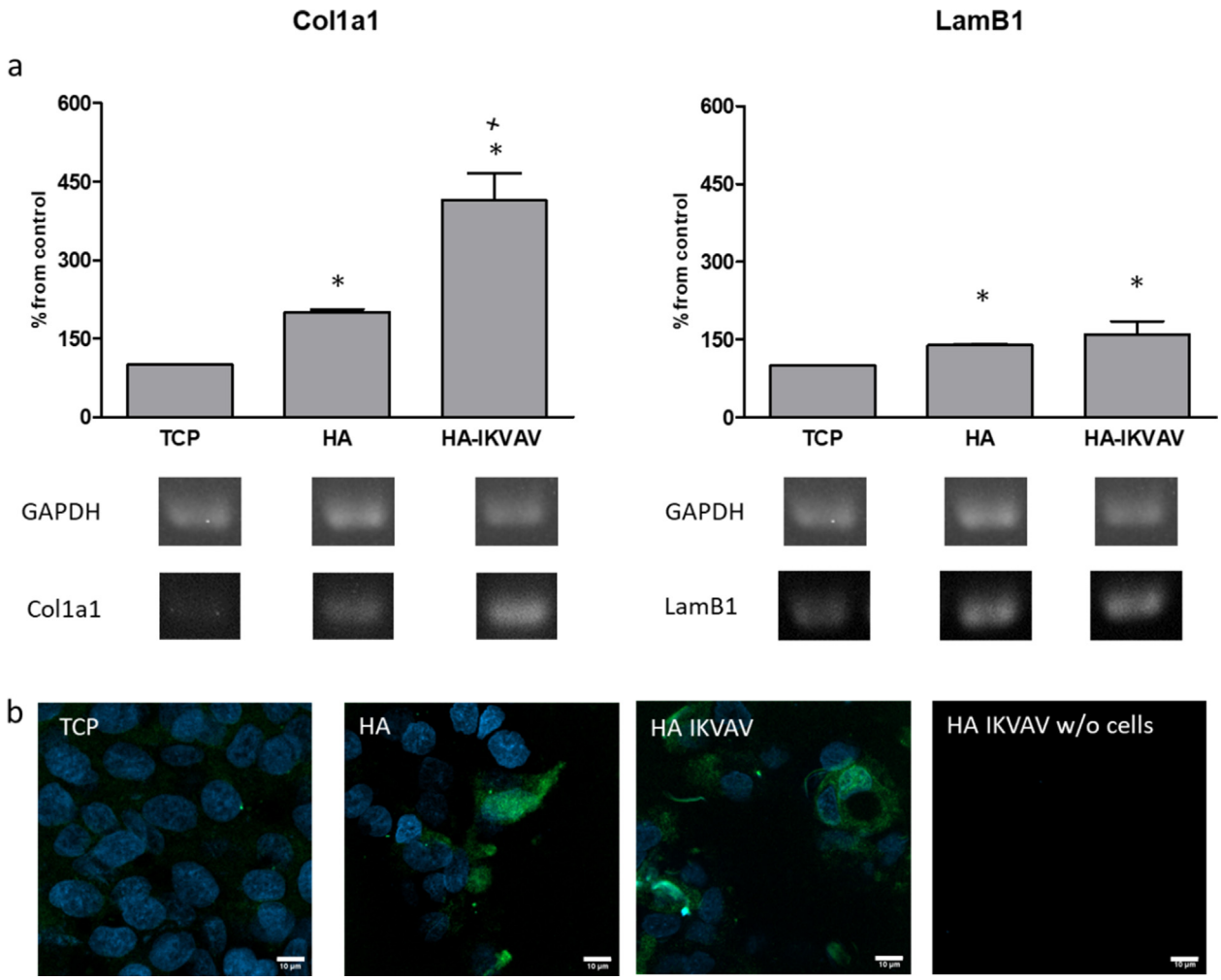

Fig. 6. RT-PCR analysis of Col1a1, and LamB1 of cultures grown on tissue-culture polystyrene (TCP), HA, and HA-IKVAV scaffolds at 3 d from seeding (a). Quantification of transcript levels was carried out by densitometric analysis using ImageLab software. Data were reported as percentage from TCP taken as 100. * = $p < 0.05$ vs TCP cultures; x = $p < 0.05$ vs cultures grown on HA; Student's *t* test. Immunofluorescence of LamB1 (b). Nuclei and LamB1-positive areas are blue and green, respectively (bar 10 μM). (For interpretation of the references to colour in this figure legend, the reader is referred to the web version of this article.)

2.5. Immunofluorescence

Air-dried slides of cell cultures were fixed in 10% buffered formalin (Sigma-Aldrich) for 15 min at 4 °C. The inactivation of non-specific binding sites was achieved by incubation with 3% BSA in phosphate buffer (PBS) for 1 h at room temperature (RT). Then, slides were incubated overnight at 4 °C with primary non-conjugate mouse monoclonal antibody anti-laminin B1 sc-374015 diluted 1:50 in 3% BSA. This antibody is specific for an epitope located between amino acids 559–586 at the C-terminus of laminin B1. Then after, samples were incubated for 30 min at RT with secondary antibody goat anti-mouse Alexa 488 diluted 1:200 in 1.5% BSA. Slides were mounted with Fluoroshield with DAPI mounting medium. Negative controls were stained by omitting the primary antibody.

2.6. Electroporation

EP of cell suspension, and cell cultures on tissue-culture polystyrene and HA-based scaffolds was performed using the voltage pulse generator EPS-01 (Igea S.p.A, Carpi, Italy). The voltage pulses were applied using a stainless steel two plates electrode (plates had a side 10 mm long with a gap of 7 mm and they were 30 mm long). Each sample was treated by means of 8 rectangular voltage pulses at 5 kHz (pulse length 100 μs, period 200 μs) with a suitable amplitude [3,4,53]. The pulse amplitude was varied between 140 and 840 V in order to generate an electric field with intensity from 400 V/cm to 1300 V/cm for electroporation curve in cell suspensions; whereas for cultures on HA-IKVAV scaffold the electric field intensity was 400, 600, 800, 1000 and 1300 V/m. EP was carried out in culture medium (RPMI) whose electrical conductivity was measured by means of Hanna Instrument electrical conductivity meter HI8883 (Hanna Instrument, Padova, Italy) calibrated at 20 °C using a standard solution, Crison conductivity standard 9710 (1413 μScm-1 @ 25 °C).

Adherent HCC1954 cells were detached with 0.25% w/v trypsin/0.53 mM EDTA solution, centrifuged, and resuspended in fresh medium at a concentration of $1x10^6$ cells/mL. Cell suspension (245 μL) was placed in each well of an 8-well Chamberslide and electroporated at different electric field intensities (0 V/cm, 400 V/cm, 600 V/cm, 800 V/cm, 1000 V/cm and 1300 V/cm). Alternatively, 8×10^5 cells were seeded on each well of an 8-well Chamberslide and electroporation was carried out at 24 h from seeding. Cell permeabilization was verified by adding 5 μL of PI (1 mg/mL in PBS) before EP. At the end of application of electric field, cells were centrifuged, and pellet was resuspended in 1 mL RPMI. Air-dried slides of cells were prepared using a Cytospin 4 (Thermo Fisher Scientific) at 500 rpm for 2 min. The slides were stained with 20 μL

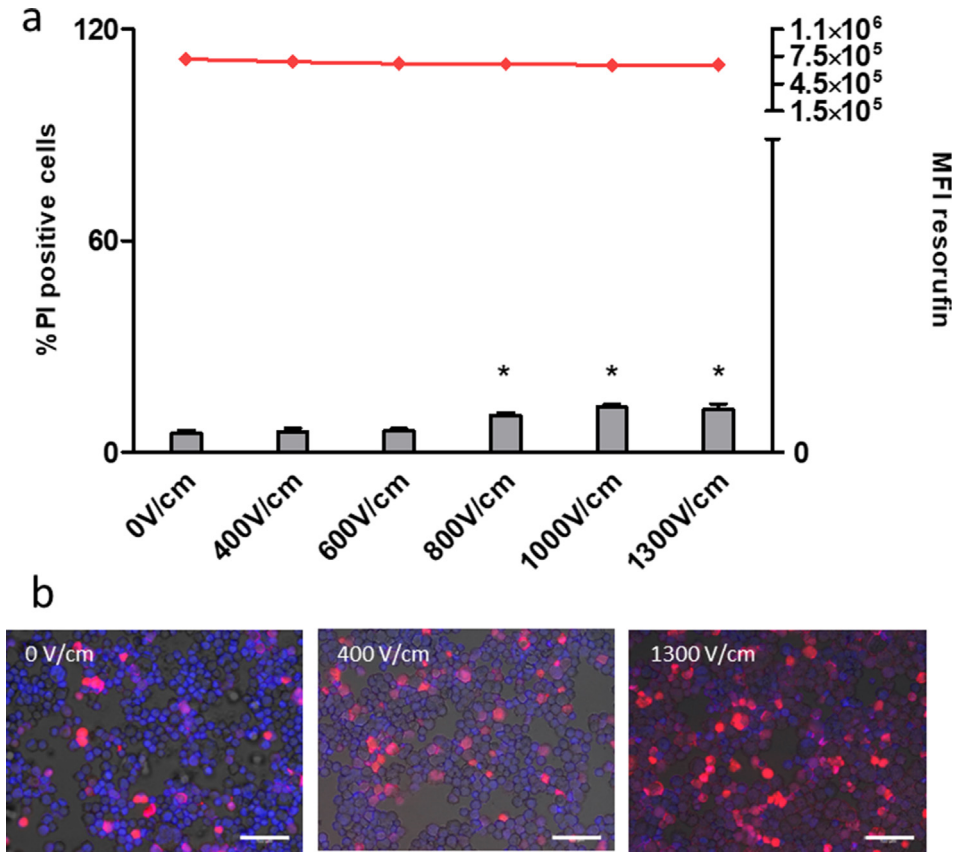

Fig. 7. Effects of EP on cell suspension. PI uptake (bars) immediately after EP and cell viability (line) at 72 h (a). * = $p < 0.05$ vs untreated cultures (0 V/cm). (b) Representative micrographs of cultures stained with PI (red) and HOE (blue). Bars: 100 μm. (For interpretation of the references to colour in this figure legend, the reader is referred to the web version of this article.)

HOE (1 mg/mL in PBS). Then, PI (excitation 538 nm, emission around 619 nm) and HOE (excitation 352 nm, emission around 455 nm) were visualized by using the fluorescence inverted microscope Leica DI4000 (objective 20x0.35 DRY, camera DFC300FXR2-078921405). Both blue and red fluorescence images were superposed to brightfield images through the software LAS AF Lite. The red (PI) and blue (HOE) images were used to evaluate the percentage of the electroporated cells as a function of the electric field intensity. The stained cells were counted in the images taken for each sample (at least 5 images per well). The percentage of red cells was evaluated for each electric field intensity applied. The experiments were repeated three times.

Cells ($2x10^5$) were also seeded on hydrated HA and HA-IKVAV scaffolds previously put in each well of an 8-well chamber slide. At 3 days from seeding, the electrode was in the well touching its bottom and 8 voltage pulses at the prescribed voltages were applied. Fig. 1 shows the chamber slide electroporation set-up with the electrode.

To verify cell permeabilization [19,54,55], 5 μL PI (1 mg/mL) and 5 μL HOE (1 mg/mL) were added to each well before and after EP, respectively. Furthermore, at 72 h from EP, cell viability was determined by Presto Blue assay as previously reported.

2.7. Statistical analysis

Data, obtained from at least three experiments, were expressed as mean ± the standard deviation of the mean. The difference between groups was evaluated using analysis of variance (ANOVA) and Student's *t*-test.

3. Results

3.1. Cell cultures on HA-based scaffolds

The synthetized scaffold observed at ESEM microscope before hydration with culture medium are shown in Fig. 2. HA-IKVAV scaffolds were characterized by a spongy structure whose holes had a minimum size close to 10 μm (average diameter 10.3 ± 3.3 μm, range 4.5–25 μm) and large surface. On the contrary, HA matrices presented a rough surface.

HCC1954 cells were seeded on HA and HA-IKVAV scaffolds and cultured for 7 d. The results were compared with those obtained on cultures grown on tissue-culture polystyrene that are often used for EP studies. Although at various degrees, spheroids were visible in all HA-based scaffolds, whereas cells formed a confluent monolayer in control cultures (Fig. 3). At 3 d from seeding, cultures on HA matrices were composed by a semiconfluent monolayer of cells and few spheroids (8 ± 4/field, diameter 48.2 ± 8.3 μm) (Fig. 3c). On HA-IKVAV cultures, spheroids, whose number increased (15 ± 2/field, diameter 45.4 ± 5.6 μm), seemed to be surrounded by both fibrous and amorphous ECM (Fig. 3e). At 7 d, in all HA-based scaffolds the cellular component appeared to be reduced: no spheroids were visible on HA, while their number (5 ± 2/field) and size (diameter 31.6 ± 7.2 μm) decreased on HA-IKVAV where the extracellular component seemed to be more abundant than those observed at 3 days (Fig. 3 d,f).

Cell viability was assessed at different time points by means of PrestoBlue assay, where the mean fluorescence intensity (MFI) is proportional to the number of viable cells. In all HA-based scaffolds cell viability was lower than that determined on tissue culture-

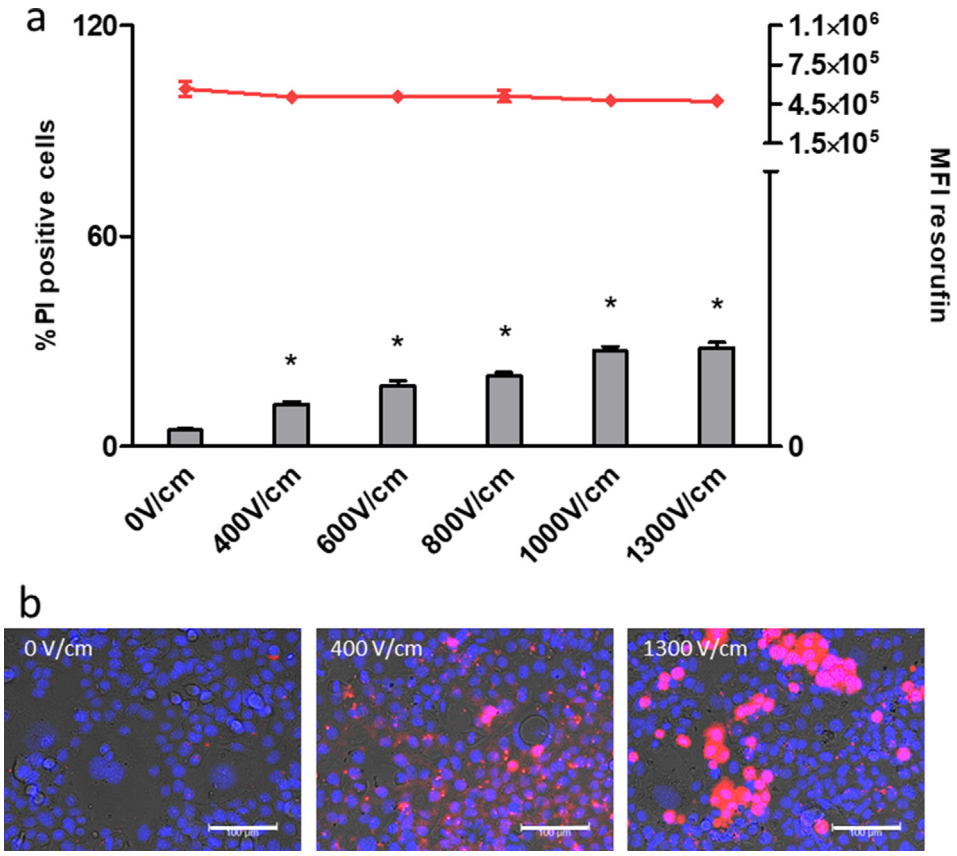

Fig. 8. Effects of EP on adherent cell cultures. PI uptake (bars) immediately after EP and cell viability (line) at 72 h (a). * = $p < 0.05$ vs untreated cultures (0 V/cm). (b) Representative micrographs of cultures stained with PI (red) and HOE (blue). Bars: 100 μm. (For interpretation of the references to colour in this figure legend, the reader is referred to the web version of this article.)

grade plastic taken as control (Fig. 4). At all time points, the MFI progressively increased in HA-IKVAV and control cultures, whereas at 7 d cell viability in HA cultures decreased compared to that detected at 3 d. Furthermore, at 1 and 3 d lower values were found in HA-IKVAV respect to HA.

To verify collagen production, the Masson's trichrome staining was carried out (Fig. 5). At 3 and 7 d, all HA-based matrices, although at various degrees, presented blue stained areas whose dimensions were quantified through image analysis. At 3 d, in HA scaffolds, the protein was organized into thin filaments that were mainly located near spheroids, whereas in HA-IKVAV a diffused and intense blue staining was noted and collagen appeared to be also organized into fibres (Fig. 5a, c). At 7 d from seeding, in both HA-based scaffolds increases in collagen-positive areas were detected. However, cultures grown on HA-IKVAV showed significantly wider blue stained areas than those found in HA cultures (Fig. 5b, d). Further experiments were carried out on cultures grown on HA-based scaffolds at 3 d from seeding, because at 7d cell viability on HA cultures decreased.

In all HA-based cultures, significant increases in both Col1a1 and LamB1 transcripts were detected than that determined in ones grown on tissue-culture polystyrene plates (Fig. 6a). Furthermore, Col1a1 levels were significantly higher in cultures grown on HA-IKVAV respect to those cultured on HA. Immunofluorescence revealed that LamB1 was also expressed as protein in HA-based cultures (Fig. 6b).

3.2. Electroporation of cell cultures

EP was carried out on cell in suspension, cultures grown on tissue-culture polystyrene plates and HA-based scaffolds by applying increasing electric fields. In untreated cultures (0 V/cm) only electrode was inserted, and no electric field was applied. The effects of electric field exposure were verified by assessing cell membrane permeabilization through PI staining immediately after EP and cell viability at 72 h from the treatment (Figs. 7-10). In cell suspensions, PI uptake significantly increased starting from 800 V/cm, whereas cell viability was not modified (Fig. 7). On the contrary, in cell cultures grown on tissue-culture polystyrene plates and HA-based scaffolds, PI uptake was enhanced at 400 V/cm (Figs. 8-10). However, in adherent cultures and HA scaffolds, at 1300 V/cm the percentages of PI positive cells were 28% and 55%, respectively. On the other hand, this value reached 90% in HA-IKVAV cultures (Fig. 10). In HA-based scaffolds, cell viability was significantly reduced when 1000 and 1300 V/cm were applied, whereas it was not affected in adherent cell cultures.

4. Discussion

Although animal models have been extensively used for anti-cancer drug discovery and development, they are ethically controversial and often unable to predict the toxicity and/or the effectiveness of chemicals in humans due to species specificity. So far, several efforts have been devoted to obtain *in vitro* culture systems. Three-dimensional *in vitro* models seem to be more representative of the tumour environment respect to 2D cultures. Indeed, this latest culture system lacks ECM, a critical component of the tumour microenvironment, produced by both stromal and cancer cells during cancer progression [56]. ECM modulates cell behaviour affecting survival, proliferation, differentiation, migration, neo-vessel formations as well as the responsiveness of cancer cells to drugs.

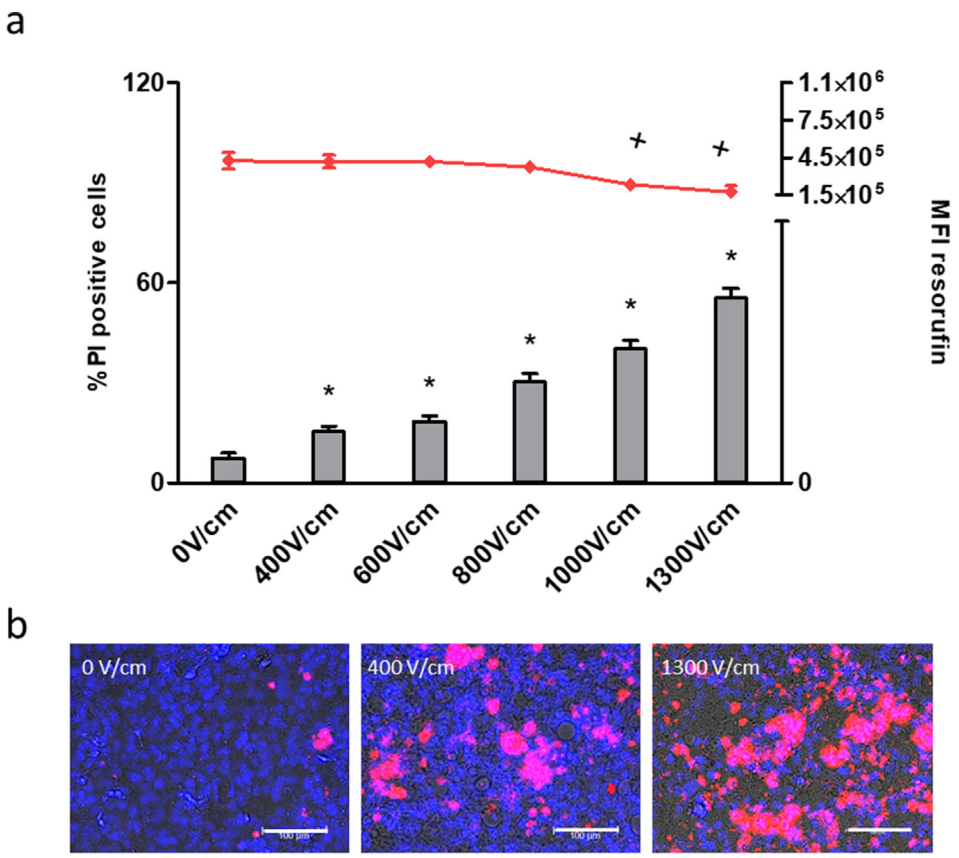

Fig. 9. Effects of EP on cultures grown on HA-based scaffolds. PI uptake (bars) immediately after EP and cell viability (line) at 72 h (a). ^{x} and * = $p < 0.05$ vs untreated cultures (0 V/cm). (b) Representative micrographs of cultures stained with PI (red) and HOE (blue). Bars: 100 μm. (For interpretation of the references to colour in this figure legend, the reader is referred to the web version of this article.)

Herein, a 3D *in vitro* model of breast cancer, overcoming the lack of an organized ECM experienced in MCTSs, is presented. To mimic the fibrous protein network filled with glycosaminoglycan hydrogel characteristic of natural ECM, semi-synthetic hydrogels consisting of HA and SAPs carrying IKVAV adhesion sequence were obtained. High amounts of HA have been found in tumor microenvironment where its interaction with cell surface receptors, such as CD44, sustains tumour progression [57]. HA-based scaffolds have already been used to form hydrogels tissue for MCTSs production [25], investigating mechanisms involved in malignant invasion [58], as well as in cancer cell line sensitivity to antimitotic drugs [59]. IKVAV, a small peptide located on the α1 chain of basement membrane glycoprotein laminin-111, promotes not only cell adhesion, but also induces tumour growth, metastasis, activation/secretion of proteases and angiogenesis [51]. These effects seem to be mediated by two integrins, α3β1 and α6β1, leading to the activation of extracellular signal-regulated kinase (ERK) 1/2 signalling.

Our data have shown that all HA-based scaffolds allowed the formation of 3D cultures where breast cancer cells organized themselves to form not only monolayer but also spheroids. Furthermore, in HA-based cultures cells were embedded in an extracellular environment provided by both scaffold and molecules synthesized and secreted by cancer cells, as already demonstrated by histological cross-sections reported in our previous work [60]. Image analysis of Masson's stained cultures revealed an enhanced collagen deposition in all HA-based cultures. Interestingly, HA-IKVAV cultures presented significantly broader positive areas than that measured in HA cultures. Histochemical data were confirmed by the increases in Col1a1 transcripts detected by means of RT-PCR. Collagen, the major structural ECM protein in tumour tissue, represents a valuable marker associated with poor survival in human breast carcinoma [61]. It may protect cancer cells from apoptosis induced by chemotherapy through activation of the PI3k/AKT pathway [62]. In particular, Col1a1 has been identified as cancer stromal genes associated with breast cancer invasion and metastasis [63].

In HA-based cultures, LamB1 was also over-expressed, as demonstrated by RT-PCR and immunofluorescence. LamB1, whose expression levels are enhanced in breast cancer, belongs to laminins, glycoproteins usually present in the basement membrane; some of them have been involved in tumour angiogenesis, invasion and metastasis [64]. Despite the formation of ECM, in HA-based cultures cell viability was significantly lower than in adherent cell cultures. This may be due to a different growth pattern: in 2D cultures cells receive nutrients and oxygen at the same extent and cover all culture surface, while in 3D system spheroid formation might lead to death of cells located in the central part of spheroids as consequence of an insufficient nutrient delivery.

Conflicting results about the influence of conductivity on EP efficiency have been reported [65]. As consequence of different experimental conditions, some papers have suggested that lower conductivities were more efficient, whereas other studies have indicated an opposite relation or no effects. Our data indicate that cell response to voltage pulse application in terms of cell membrane permeabilization may depend, at least in part, on the surrounding environment. In cell suspension, the percentage of PI positive cells was lower (about 20%) than that obtained (90–100%) by other researchers using EP buffer that shows a conductivity of 0.14 S/m [14,17,18,55,66–68]. This discrepancy can be due to medium conductivity because in this work EP was carried out in

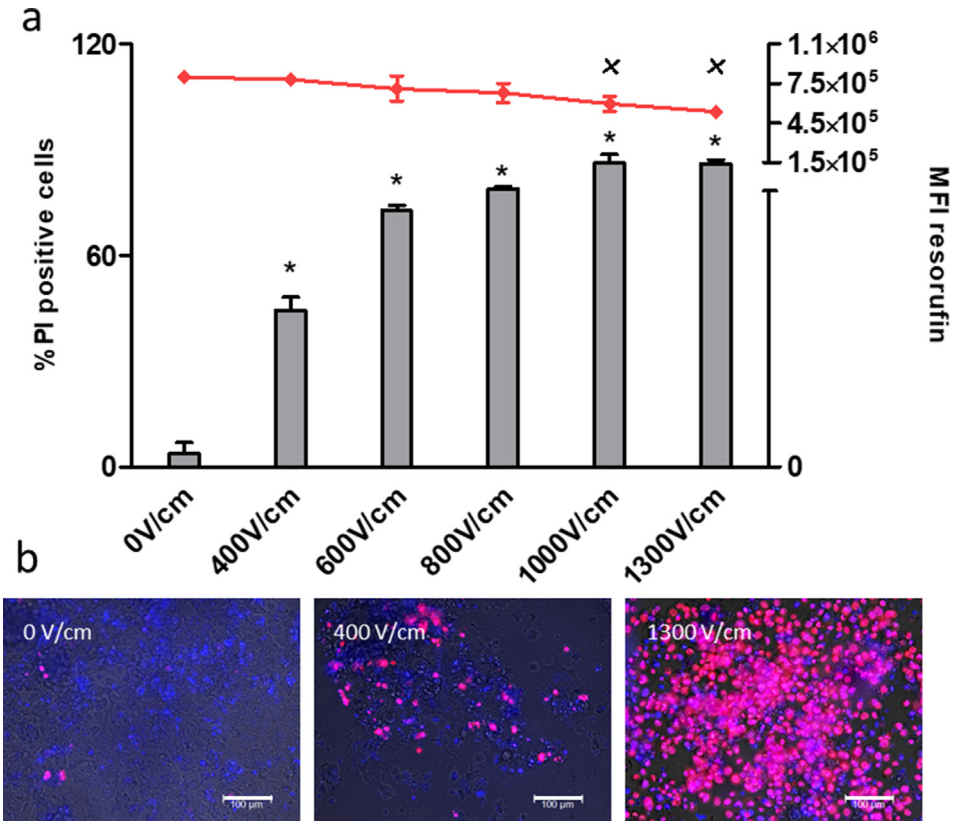

Fig. 10. Effects of EP on cultures grown on HA-IKVAV-based scaffolds. PI uptake (bars) immediately after EP and cell viability (line) at 72 h (a). ^{x} and * = $p < 0.05$ vs untreated cultures (0 V/cm). (b) Representative micrographs of cultures stained with PI (red) and HOE (blue). Bars: 100 μm. (For interpretation of the references to colour in this figure legend, the reader is referred to the web version of this article.)

culture medium that shows a conductivity of 1.3 S/m and not in EP buffer. Herein, PI uptake progressively increased starting from cell in suspension, lacking ECM, to adherent cell and HA-based cultures, characterized by different ECM deposition. Above all, cell permeabilization on HA-IKVAV, where collagen production was higher than those detected in the other culture conditions, was enhanced: the percentage of PI positive cells was about 50 and 90% at 400 V/cm and 1300 V/cm, respectively. Furthermore, EP efficiency may depend also on shape and size of the cells and their orientation with respect to the direction of the electric field for elongated cells [2,69].

At 3 d from EP, reductions in cell viability were observed by increasing the intensity of the applied electric field in HA-based scaffolds, whereas no variations were detected in cell in suspension and adherent cell cultures. This different behavior may be related to the electric field distribution which depends on inhomogeneous conductivity of the environment surrounding the cells, as highlighted by numerical models and experimental phantoms [70]. In HA-based cultures, local increases in the electric field due to the presence of collagen (conductivity close to 0.2 S/m) may co-exist with areas where culture medium conductivity (1.3 S/m) prevails. Thus, the electric field may locally reach the irreversible electroporation threshold inducing cell death [71–73].

5. Conclusions

Collectively, our data suggest that HA-IKVAV cultures may represent an interesting model for EP studies. The enrichment of HA scaffolds with IKVAV motif modulates cell viability, cell organization and ECM production. Indeed, increases in spheroid number, ECM formation and Col1a1 transcripts were detected in cultures grown on HA-IKVAV respect to those on HA.

Cell sensitivity to EP seemed to be modulated by the presence of ECM and the different cell organization. Cell permeabilization progressively increased ranging from 2D cultures to 3D HA-based cultures: the highest values of PI uptake were detected in HA-IKVAV cultures characterized by abundant ECM production. Although in our 3D model a relationship between cell permeabilization and environment conductivity have been supposed, further studies will be needed to elucidate the influence of ECM composition on EP efficiency.

Declaration of Competing Interest

The authors declare that they have no known competing financial interests or personal relationships that could have appeared to influence the work reported in this paper.

Acknowledgments

Authors are grateful to Igea S.p.A. (Carpi, Italy) for pulse generator and electrodes, to Dr. Claudio Furlan for ESEM images, to Stefano Centenaro for his help in scaffolds preparation, and to Davide Albertini for the image analysis. Project was granted by CPDA138001 (Padua University) and partially by COST TD1104 action (www.electroporation.net).

References

[1] L.M. Mir, Therapeutic perspectives of in vivo cell electropermeabilization, Bioelectrochemistry 53 (2001) 1–10, https://doi.org/10.1016/S0302-4598(00)00112-4.

[2] T. Kotnik, P. Kramar, G. Pucihar, D. Miklavcic, M. Tarek, Cell membrane electroporation- Part 1: The phenomenon, IEEE Electr. Insul. Mag. 28 (2012) 14–23, https://doi.org/10.1109/MEI.2012.6268438.

[3] M. Marty, G. Sersa, J.R. Garbay, J. Gehl, C.G. Collins, M. Snoj, V. Billard, P.F. Geertsen, J.O. Larkin, D. Miklavcic, I. Pavlovic, S.M. Paulin-Kosir, M. Cemazar, N. Morsli, D.M. Soden, Z. Rudolf, C. Robert, G.C. O'Sullivan, L.M. Mir, Electrochemotherapy – An easy, highly effective and safe treatment of cutaneous and subcutaneous metastases: Results of ESOPE (European Standard Operating Procedures of Electrochemotherapy) study, Eur. J. Cancer Suppl. 4 (2006) 3–13, https://doi.org/10.1016/j.ejcsup.2006.08.002.

[4] L.M. Mir, J. Gehl, G. Sersa, C.G. Collins, J.-R. Garbay, V. Billard, P.F. Geertsen, Z. Rudolf, G.C. O'Sullivan, M. Marty, Standard operating procedures of the electrochemotherapy: Instructions for the use of bleomycin or cisplatin administered either systemically or locally and electric pulses delivered by the CliniporatorTM by means of invasive or non-invasive electrodes, EJC Supplements 4 (2006) 14–25.

[5] L. Campana, S. Mocellin, M. Basso, O. Puccetti, G. De Salvo, V. Chiarion-Sileni, A. Vecchiato, L. Corti, C. Rossi, D. Nitti, Bleomycin-based electrochemotherapy: clinical outcome from a single institution's experience with 52 patients, Ann. Surg. Oncol. 16 (2009) 191–199, https://doi.org/10.1245/s10434-008-0204-8.

[6] N. Mozzillo, C. Caraco, S. Mori, G. Di Monta, G. Botti, P. Ascierto, C. Caraco, L. Aloj, Use of neoadjuvant electrochemotherapy to treat a large metastatic lesion of the cheek in a patient with melanoma, J. Trans. Med. 10 (2012) 131.

[7] G. Sersa, T. Cufer, S.M. Paulin, M. Cemazar, M. Snoj, Electrochemotherapy of chest wall breast cancer recurrence, Cancer Treat. Rev. 38 (2012) 379–386, https://doi.org/10.1016/j.ctrv.2011.07.006.

[8] D. Miklavčič, G. Serša, E. Brecelj, J. Gehl, D. Soden, G. Bianchi, P. Ruggieri, C.R. Rossi, L.G. Campana, T. Jarm, Electrochemotherapy: technological advancements for efficient electroporation-based treatment of internal tumors, Med. Biol. Eng. Comput. 50 (2012) 1213–1225, https://doi.org/10.1007/s11517-012-0991-8.

[9] I. Edhemovic, E. Brecelj, G. Gasljevic, M. Marolt Music, V. Gorjup, B. Mali, T. Jarm, B. Kos, D. Pavliha, B. Grcar Kuzmanov, M. Cemazar, M. Snoj, D. Miklavcic, E.M. Gadzijev, G. Sersa, Intraoperative electrochemotherapy of colorectal liver metastases, J. Surg. Oncol. 110 (2014) 320–327, https://doi.org/10.1002/jso.23625.

[10] G. Sersa, D. Miklavcic, M. Cemazar, Z. Rudolf, G. Pucihar, M. Snoj, Electrochemotherapy in treatment of tumours, Europ. J. Surg. Oncol. (EJSO) 34 (2008) 232–240, https://doi.org/10.1016/j.ejso.2007.05.016.

[11] I. Edhemovic, E.M. Gadzijev, E. Brecelj, D. Miklavcic, B. Kos, A. Zupanic, B. Mali, T. Jarm, D. Pavliha, M. Marcan, G. Gasljevic, V. Gorjup, M. Music, T.P. Vavpotic, M. Cemazar, M. Snoj, G. Sersa, Electrochemotherapy: a new technological approach in treatment of metastases in the liver, Technol. Cancer Res. Treat. 10 (2011) 475–485.

[12] G. Bianchi, L. Campanacci, M. Ronchetti, D. Donati, Electrochemotherapy in the treatment of bone metastases: a phase II trial, World J. Surg. 40 (2016) 3088–3094, https://doi.org/10.1007/s00268-016-3627-6.

[13] D. Miklavčič, Handbook of electroporation, 2016. http://link.springer.com/referencework/10.1007/978-3-319-26779-1 (accessed June 20, 2017).

[14] M. Pavlin, M. Kandušer, M. Reberšek, G. Pucihar, F.X. Hart, R. Magjarevićcacute, D. Miklavčič, Effect of cell electroporation on the conductivity of a cell suspension, Biophys. J. 88 (2005) 4378–4390, https://doi.org/10.1529/biophysj.104.048975.

[15] W. Korohoda, M. Grys, Z. Madeja, Reversible and irreversible electroporation of cell suspensions flowing through a localized DC electric field, Cell. Mol. Biol. Lett. 18 (2013) 102–119, https://doi.org/10.2478/s11658-012-0042-3.

[16] G. Pucihar, T. Kotnik, J. Teissié, D. Miklavčič, Electropermeabilization of dense cell suspensions, Eur. Biophys. J. 36 (2007) 173–185.

[17] P. Ruzgys, M. Jakutavičiūtė, I. Šatkauskienė, K. Čepurnienė, S. Šatkauskas, Effect of electroporation medium conductivity on exogenous molecule transfer to cells in vitro, Sci. Rep. 9 (2019) 1436, https://doi.org/10.1038/s41598-018-38287-8.

[18] S. Šatkauskas, B. Jakštys, P. Ruzgys, M. Jakutavičiūtė, Different cell viability assays following electroporation in vitro, in: D. Miklavcic (Ed.), Handbook of Electroporation, Springer International Publishing, Cham, 2016, pp. 1–14, https://doi.org/10.1007/978-3-319-26779-1_140-1.

[19] T. Batista Napotnik, D. Miklavčič, In vitro electroporation detection methods – An overview, Bioelectrochemistry 120 (2018) 166–182, https://doi.org/10.1016/j.bioelechem.2017.12.005.

[20] A. Ben-Ze'ev, G.S. Robinson, N.L. Bucher, S.R. Farmer, Cell-cell and cell-matrix interactions differentially regulate the expression of hepatic and cytoskeletal genes in primary cultures of rat hepatocytes, Proc. Natl. Acad. Sci. 85 (1988) 2161–2165, https://doi.org/10.1073/pnas.85.7.2161.

[21] S.A. Lelièvre, T. Kwok, S. Chittiboyina, Architecture in 3D cell culture: An essential feature for in vitro toxicology, Toxicol. In Vitro 45 (2017) 287–295, https://doi.org/10.1016/j.tiv.2017.03.012.

[22] J. Saji Joseph, S. Tebogo Malindisa, M. Ntwasa, Two-Dimensional (2D) and Three-Dimensional (3D) Cell Culturing in Drug Discovery, in: R. Ali Mehanna (Ed.), Cell Culture, IntechOpen, 2019. https://doi.org/10.5772/intechopen.81552.

[23] F. Pampaloni, E.H.K. Stelzer, A. Masotti, Three-dimensional tissue models for drug discovery and toxicology, Recent Pat Biotechnol. 3 (2009) 103–117.

[24] S. Ceylan, N. Bolgen, A review on three dimensional scaffolds for tumor engineering, Biomater. Biomech. Bioeng. 3 (2016) 141–155, https://doi.org/10.12989/BME.2016.3.3.141.

[25] M.P. Carvalho, E.C. Costa, S.P. Miguel, I.J. Correia, Tumor spheroid assembly on hyaluronic acid-based structures: A review, Carbohydr. Polym. 150 (2016) 139–148, https://doi.org/10.1016/j.carbpol.2016.05.005.

[26] J. Insua-Rodríguez, T. Oskarsson, The extracellular matrix in breast cancer, Adv. Drug Deliv. Rev. 97 (2016) 41–55, https://doi.org/10.1016/j.addr.2015.12.017.

[27] M. Pavlin, N. Pavselj, D. Miklavcic, Dependence of induced transmembrane potential on cell density, arrangement, and cell position inside a cell system, IEEE Trans. Biomed. Eng. 49 (2002) 605–612, https://doi.org/10.1109/TBME.2002.1001975.

[28] A. Bernardis, M. Bullo, L.G. Campana, P. Di Barba, F. Dughiero, M. Forzan, M.E. Mognaschi, P. Sgarbossa, E. Sieni, Electric field computation and measurements in the electroporation of inhomogeneous samples, Open Phys. 15 (2017), https://doi.org/10.1515/phys-2017-0092.

[29] M. Kranjc, F. Bajd, I. Sersa, D. Miklavcic, Magnetic resonance electrical impedance tomography for monitoring electric field distribution during tissue electroporation, IEEE Trans. Med. Imaging 30 (2011) 1771–1778, https://doi.org/10.1109/TMI.2011.2147328.

[30] L.G. Campana, Di Barba Paolo, M.E. Mognaschi, M. Bullo, F. Dughiero, M. Forzan, P. Sgarbossa, E. Spessot, E. Sieni, Electrical resistance in inhomogeneous samples during electroporation, Proc. SMACD (2017).

[31] E.C. Costa, A.F. Moreira, D. de Melo-Diogo, V.M. Gaspar, M.P. Carvalho, I.J. Correia, 3D tumor spheroids: an overview on the tools and techniques used for their analysis, Biotechnol. Adv. 34 (2016) 1427–1441, https://doi.org/10.1016/j.biotechadv.2016.11.002.

[32] K. Brajša, Three-dimensional cell cultures as a new tool in drug discovery, Period. Biol. 118 (2016) 59–65, https://doi.org/10.18054/pb.2016.118.1.3940.

[33] F. Pampaloni, E. Stelzer, Three-dimensional cell cultures in toxicology, Biotechnol. Genet. Eng. Rev. 26 (2010) 117–138.

[34] L. Gibot, L. Wasungu, J. Teissié, M.-P. Rols, Antitumor drug delivery in multicellular spheroids by electropermeabilization, J. Control. Release 167 (2013) 138–147, https://doi.org/10.1016/j.jconrel.2013.01.021.

[35] L. Gibot, M. Madi, R. Vézinet, M.P. Rols, Mixed spheroids as a relevant 3D biological tool to understand therapeutic window of electrochemotherapy, in: T. Jarm, P. Kramar (Eds.), 1st World Congress on Electroporation and Pulsed Electric Fields in Biology, Medicine and Food & Environmental Technologies, Springer, Singapore, 2016, pp. 200–203, https://doi.org/10.1007/978-981-287-817-5_45.

[36] H.R. Mellor, L.A. Davies, H. Caspar, C.R. Pringle, S.C. Hyde, D.R. Gill, R. Callaghan, Optimising non-viral gene delivery in a tumour spheroid model, J. Gene Med. 8 (2006) 1160–1170, https://doi.org/10.1002/jgm.947.

[37] L.P. Ferreira, V.M. Gaspar, J.F. Mano, Design of spherically structured 3D in vitro tumor models - advances and prospects, Acta Biomater. 75 (2018) 11–34, https://doi.org/10.1016/j.actbio.2018.05.034.

[38] C.B. Arena, C.S. Szot, P.A. Garcia, M.N. Rylander, R.V. Davalos, A three-dimensional in vitro tumor platform for modeling therapeutic irreversible electroporation, Biophys. J. 103 (2012) 2033–2042, https://doi.org/10.1016/j.bpj.2012.09.017.

[39] M. Dettin, A. Zamuner, M. Roso, A. Gloria, G. Iucci, G.M.L. Messina, U. D'Amora, G. Marletta, M. Modesti, I. Castagliuolo, P. Brun, Electrospun scaffolds for osteoblast cells: peptide-induced concentration-dependent improvements of polycaprolactone, PLoS ONE 10 (2015), https://doi.org/10.1371/journal.pone.0137505 e0137505.

[40] A.A. Bulysheva, R. Heller, 3D culture models to assess tissue responses to electroporation, in: D. Miklavcic (Ed.), Handbook of Electroporation, Springer International Publishing, Cham, 2017, pp. 1–14, https://doi.org/10.1007/978-3-319-26779-1_29-1.

[41] A.A. Bulysheva, N. Burcus, C. Lundberg, C.M. Edelblute, M.P. Francis, R. Heller, Recellularized human dermis for testing gene electrotransferex vivo, Biomed. Mater. 11 (2016), https://doi.org/10.1088/1748-6041/11/3/035002 035002.

[42] S. Pradhan, I. Hassani, J.M. Clary, E.A. Lipke, Polymeric biomaterials for in vitro cancer tissue engineering and drug testing applications, Tissue Eng. Part B: Rev. 22 (2016) 470–484, https://doi.org/10.1089/ten.teb.2015.0567.

[43] P.J. Canatella, M.M. Black, D.M. Bonnichsen, C. McKenna, M.R. Prausnitz, Tissue electroporation: quantification and analysis of heterogeneous transport in multicellular environments, Biophys. J. 86 (2004) 3260–3268, https://doi.org/10.1016/S0006-3495(04)74374-X.

[44] M. Madi, M.-P. Rols, L. Gibot, Gene electrotransfer in 3D reconstructed human dermal tissue, Curr. Gene Ther. 16 (2016) 75–82.

[45] B. Marrero, R. Heller, The use of an in vitro 3D melanoma model to predict in vivo plasmid transfection using electroporation, Biomaterials 33 (2012) 3036–3046, https://doi.org/10.1016/j.biomaterials.2011.12.049.

[46] M. Madi, M.-P. Rols, L. Gibot, Efficient in vitro electropermeabilization of reconstructed human dermal tissue, J. Membrane Biol. 248 (2015) 903–908, https://doi.org/10.1007/s00232-015-9791-z.

[47] P. Brun, M. Dettin, L.G. Campana, F. Dughiero, P. Sgarbossa, C. Bernardello, A.L. Tosi, A. Zamuner, E. Sieni, Cell-seeded 3D scaffolds as in vitro models for electroporation, Bioelectrochemistry 125 (2019) 15–24, https://doi.org/10.1016/j.bioelechem.2018.08.006.

[48] Dettin, Sieni, Zamuner, Marino, Sgarbossa, Lucibello, Tosi, Keller, Campana, Signori, A novel 3D scaffold for cell growth to assess electroporation efficacy, Cells 8 (2019) 1470. https://doi.org/10.3390/cells8111470.

[49] S. Zhang, Emerging biological materials through molecular self-assembly, Biotechnol. Adv. 20 (2002) 321–339, https://doi.org/10.1016/S0734-9750(02)00026-5.

[50] S. Zhang, T. Holmes, C. Lockshin, A. Rich, Spontaneous assembly of a self-complementary oligopeptide to form a stable macroscopic membrane, Proc. Natl. Acad. Sci. USA 90 (1993) 3334–3338.
[51] Y. Kikkawa, K. Hozumi, F. Katagiri, M. Nomizu, H.K. Kleinman, J.E. Koblinski, Laminin-111-derived peptides and cancer, Cell Adhes. Migrat. 7 (2013) 150–159, https://doi.org/10.4161/cam.22827.
[52] A. Zamuner, M. Cavo, S. Scaglione, G. Messina, T. Russo, A. Gloria, G. Marletta, M. Dettin, Design of decorated self-assembling peptide hydrogels as architecture for mesenchymal stem cells, Materials 9 (2016) 727, https://doi.org/10.3390/ma9090727.
[53] A. Ongaro, L.G. Campana, M. De Mattei, F. Dughiero, M. Forzan, A. Pellati, C.R. Rossi, E. Sieni, Evaluation of the electroporation efficiency of a grid electrode for electrochemotherapy: from numerical model to in vitro tests, Technol. Cancer Res. Treat. 15 (2016) 296–307, https://doi.org/10.1177/1533034615582350.
[54] J.A. Steinkamp, B.E. Lehnert, N.M. Lehnert, Discrimination of damaged/dead cells by propidium iodide uptake in immunofluorescently labeled populations analyzed by phase-sensitive flow cytometry, J. Immunol. Methods 226 (1999) 59–70, https://doi.org/10.1016/S0022-1759(99)00053-8.
[55] T.B. Napotnik, Fluorescent indicators of membrane permeabilization due to electroporation, in: D. Miklavcic (Ed.), Handbook of Electroporation, Springer International Publishing, Cham, 2016, pp. 1–19, https://doi.org/10.1007/978-3-319-26779-1_133-1.
[56] A. Naba, K.R. Clauser, J.M. Lamar, S.A. Carr, R.O. Hynes, Extracellular matrix signatures of human mammary carcinoma identify novel metastasis promoters, ELife. 3 (2014), https://doi.org/10.7554/eLife.01308 e01308.
[57] P. Auvinen, R. Tammi, J. Parkkinen, M. Tammi, U. Ågren, R. Johansson, P. Hirvikoski, M. Eskelinen, V.-M. Kosma, Hyaluronan in peritumoral stroma and malignant cells associates with breast cancer spreading and predicts survival, Am. J. Pathol. 156 (2000) 529–536, https://doi.org/10.1016/S0002-9440(10)64757-8.
[58] L. David, V. Dulong, D. Le Cerf, C. Chauzy, V. Norris, B. Delpech, M. Lamacz, J.-P. Vannier, Reticulated hyaluronan hydrogels: a model for examining cancer cell invasion in 3D, Matrix Biol. 23 (2004) 183–193, https://doi.org/10.1016/j.matbio.2004.05.005.
[59] L. David, V. Dulong, D. Le Cerf, L. Cazin, M. Lamacz, J.-P. Vannier, Hyaluronan hydrogel: An appropriate three-dimensional model for evaluation of anticancer drug sensitivity, Acta Biomater. 4 (2008) 256–263, https://doi.org/10.1016/j.actbio.2007.08.012.
[60] E. Sieni, M. Dettin, M. De Robertis, B. Bazzolo, M.T. Conconi, A. Zamuner, R. Marino, F. Keller, L.G. Campana, E. Signori, The efficiency of gene electrotransfer in breast-cancer cell lines cultured on a novel collagen-free 3D scaffold, Cancers. 12 (2020) 1043, https://doi.org/10.3390/cancers12041043.
[61] M.W. Conklin, J.C. Eickhoff, K.M. Riching, C.A. Pehlke, K.W. Eliceiri, P.P. Provenzano, A. Friedl, P.J. Keely, Aligned collagen is a prognostic signature for survival in human breast carcinoma, Am. J. Pathol. 178 (2011) 1221–1232, https://doi.org/10.1016/j.ajpath.2010.11.076.
[62] T. Hoshiba, M. Tanaka, Breast cancer cell behaviors on staged tumorigenesis-mimicking matrices derived from tumor cells at various malignant stages, Biochem. Biophys. Res. Commun. 439 (2013) 291–296, https://doi.org/10.1016/j.bbrc.2013.08.038.
[63] Y. Wang, H. Xu, B. Zhu, Z. Qiu, Z. Lin, Systematic identification of the key candidate genes in breast cancer stroma, Cell Mol. Biol. Lett. 23 (2018) 44, https://doi.org/10.1186/s11658-018-0110-4.
[64] Y. Qin, S. Rodin, O.E. Simonson, F. Hollande, Laminins and cancer stem cells: Partners in crime?, Semin. Cancer Biol. 45 (2017) 3–12, https://doi.org/10.1016/j.semcancer.2016.07.004.
[65] A. Silve, I. Leray, C. Poignard, L.M. Mir, Impact of external medium conductivity on cell membrane electropermeabilization by microsecond and nanosecond electric pulses, Sci Rep. 6 (2016) 19957, https://doi.org/10.1038/srep19957.
[66] A. Ongaro, A. Pellati, A. Caruso, M. Battista, F. De Terlizzi, M. De Mattei, M. Fini, Identification of in vitro electropermeabilization equivalent pulse protocols, Technol. Cancer Res. Treat. 10 (2011) 465–473.
[67] J. Dermol, D. Miklavčič, Predicting electroporation of cells in an inhomogeneous electric field based on mathematical modeling and experimental CHO-cell permeabilization to propidium iodide determination, Bioelectrochemistry 100 (2014) 52–61, https://doi.org/10.1016/j.bioelechem.2014.03.011.
[68] G. Pucihar, L.M. Mir, D. Miklavcic, The effect of pulse repetition frequency on the uptake into electropermeabilized cells in vitro with possible applications in electrochemotherapy, Bioelectrochemistry 57 (2002) 167–172.
[69] D. Miklavčič, N. Pavšelj, F.X. Hart, Electric properties of tissues, in: Wiley Encyclopedia of Biomedical Engineering, John Wiley & Sons, Inc., 2006. http://dx.doi.org/10.1002/9780471740360.ebs0403.
[70] L.G. Campana, M. Bullo, P. Di Barba, F. Dughiero, M. Forzan, M.E. Mognaschi, P. Sgarbossa, A.L. Tosi, A. Bernardis, E. Sieni, Effect of tissue inhomogeneity in soft tissue sarcomas: from real cases to numerical and experimental models, Technol. Cancer Res. Treat. 17 (2018), https://doi.org/10.1177/1533033818789693, 153303381878969.
[71] D. Miklavcic, R.V. Davalos, Electrochemotherapy (ECT) and irreversible electroporation (IRE) -advanced techniques for treating deep-seated tumors based on electroporation, Biomed Eng Online. 14 (2015) I1, https://doi.org/10.1186/1475-925X-14-S3-I1.
[72] A. Nickfarjam, S.M.P. Firoozabadi, Parametric study of irreversible electroporation with different needle electrodes: Electrical and thermal analysis, Int. J. Hyperth. 30 (2014) 335–347, https://doi.org/10.3109/02656736.2014.937775.
[73] B. Rubinsky, Irreversible electroporation, Springer, Berlin, Heidelberg, 2010.